PNAS RESEARCH ARTICLE | NEUROSCIENCE
BIOPHYSICS AND COMPUTATIONAL BIOLOGY

Genetic mechanisms for impaired synaptic plasticity in schizophrenia revealed by computational modeling

Tuomo Mäki-Marttunen[a,b,1], Kim T. Blackwell[c], Ibrahim Akkouh[d,e], Alexey Shadrin[d,f], Mathias Valstad[g], Torbjørn Elvsåshagen[d,h], Marja-Leena Linne[a], Srdjan Djurovic[d,e,f], Gaute T. Einevoll[i,j], and Ole A. Andreassen[d,k]

Affiliations are included on p. 11.

Edited by Terrence Sejnowski, Salk Institute for Biological Studies, La Jolla, CA; received July 21, 2023; accepted March 23, 2024

Schizophrenia phenotypes are suggestive of impaired cortical plasticity in the disease, but the mechanisms of these deficits are unknown. Genomic association studies have implicated a large number of genes that regulate neuromodulation and plasticity, indicating that the plasticity deficits have a genetic origin. Here, we used biochemically detailed computational modeling of postsynaptic plasticity to investigate how schizophrenia-associated genes regulate long-term potentiation (LTP) and depression (LTD). We combined our model with data from postmortem RNA expression studies (CommonMind gene-expression datasets) to assess the consequences of altered expression of plasticity-regulating genes for the amplitude of LTP and LTD. Our results show that the expression alterations observed post mortem, especially those in the anterior cingulate cortex, lead to impaired protein kinase A (PKA)-pathway-mediated LTP in synapses containing GluR1 receptors. We validated these findings using a genotyped electroencephalogram (EEG) dataset where polygenic risk scores for synaptic and ion channel-encoding genes as well as modulation of visual evoked potentials were determined for 286 healthy controls. Our results provide a possible genetic mechanism for plasticity impairments in schizophrenia, which can lead to improved understanding and, ultimately, treatment of the disorder.

modeling of intracellular signaling pathways | long-term potentiation (LTP) | schizophrenia | postmortem RNA expression | GWAS

Significance

Synaptic plasticity has been suggested to be impaired in schizophrenia, but mechanisms linking schizophrenia-associated genes with phenotypes expressing altered plasticity have been lacking. Here, we aimed to bridge this gap by biochemically detailed modeling of intracellular signaling pathways underlying synaptic plasticity. We combined our model with gene expression data from schizophrenia patients and healthy controls to show that the alterations observed post mortem in schizophrenia patients lead to impairments of synaptic plasticity in the cortex. Finally, we validated our predictions for the importance of synaptic plasticity-regulating genes by using a separate electroencephalogram (EEG) dataset that included the genotype of each subject: the number of schizophrenia-associated gene variants in the plasticity-regulating genes was correlated with an impaired potentiation of visual evoked potentials.

Schizophrenia (SCZ) is a severe mental disorder, characterized by negative, positive, and cognitive symptoms (1). Although some medications have proved successful in constraining the positive symptoms, few drugs help improve the negative and cognitive symptoms of SCZ (2). The mechanisms of SCZ symptoms are far from understood but it is believed that they involve impaired function at the synaptic level. Previous studies have suggested synaptic plasticity, which is a key cellular mechanism behind cognitive functions such as learning and memory, as one of the overarching cellular-level abnormalities in the disorder pathology (3–6).

Synaptic plasticity depends on the orchestrated action of a multitude of second messenger molecules and proteins. Genome-wide association studies (GWASs) have identified variants associated with risk of SCZ in hundreds of genes (7, 8), and many of these genes are fundamental for neuromodulation and synaptic plasticity (9). Conclusive experimental data on the effects of SCZ-associated variants on plasticity mechanisms is difficult to obtain due to the large number of implicated gene variants. In fact, apart from a few ultra-high-risk variants that have been studied in genetic animal models, it is not known how the variants affect plasticity either in a single neuron or at a network level. Here, we address this question by means of computational modeling of biochemical signaling pathways. Computational models provide an efficient means of assessing synaptic plasticity and exploring how it is affected by variations in the patients' genetic make-up. We used the CommonMind gene-expression datasets from postmortem brains of SCZ patients and healthy controls (HCs) (10) that provide information on whether the expression of genes, particularly those associated with risk single-nucleotide polymorphisms (SNPs), are up- or down-regulated or unaffected in SCZ. We applied a computational model (11) to the patients' brain gene expression data and investigated the effects of gene variants on the pathways that lead to long-term potentiation (LTP) and depression (LTD). In this way, we could unravel how genetic variants associated with SCZ relate to central synaptic plasticity mechanisms.

Although SCZ symptoms are difficult to study due to a lack of suitable corresponding conditions in animals in vivo, there are other robust phenotypes of SCZ that are quantifiable via electrophysiology (12). A mental disorder phenotype strongly suggestive

This article is a PNAS Direct Submission.

[1]To whom correspondence may be addressed. Email: tuomo.maki-marttunen@tuni.fi.

This article contains supporting information online at https://www.pnas.org/lookup/suppl/doi:10.1073/pnas.2312511121/-/DCSupplemental.

Published August 14, 2024.

of a deficit in synaptic plasticity is the modulation of visual evoked potential (VEP), a.k.a. LTP-like plasticity of VEP, which is impaired in SCZ patients compared to HCs (13). A specific aim of the current study was to explore how this phenotype is altered by variants of SCZ-associated genes.

Using the model of ref. 11, we explored the impact that the altered expression profile of plasticity-regulating genes, as measured in prefrontal cortices (PFC) and anterior cingulate cortices (ACC) of SCZ patients, have on several forms of synaptic plasticity. We showed that both the conventional forms of plasticity (low- and high-frequency stimulation (LFS/HFS) induced plasticity and spike-timing-dependent plasticity, STDP) and the plasticity induced by the VEP protocol are significantly impaired by the alterations of protein levels suggested by postmortem expression data and that these alterations are driven by impaired protein kinase A (PKA)-pathway-mediated synaptic potentiation. We used a genotyped dataset from a VEP modulation experiment of 286 HCs to validate our results and found that the associations between polygenic risk scores (PRSs) of SCZ based on groups of genes relevant for synaptic plasticity supported our predictions for the impairments of synaptic plasticity. Our results uncover mechanisms behind the phenotype of altered VEP modulation and help to narrow down the pathways through which cortical synaptic plasticity is impaired in SCZ.

Results

The Model Reproduces Numerous Forms of Plasticity. Synaptic plasticity in the cortex is dependent on a wide set of molecular mechanisms that vary between cortical areas and stages of development. To investigate the role of diverse pathways in different forms of plasticity affected by SCZ, we enhanced our model (11) to include neurogranin, which is critical for plasticity (14), and improved the model of GluR1 cycling (*SI Appendix, Materials and Methods*). We then validated our model (illustrated in Fig. 1*A*) by fitting the parameters to different datasets using multiobjective optimization where the quantities of different proteins were varied to match the LTP/LTD outcome observed in the experiments. We were able to reproduce all the data as in the original model (11) and found parameter sets that reproduced CaMKII- and stimulation frequency-dependent plasticity in V1 (15) in adult (*SI Appendix*, Fig. S1*A*) and young (*SI Appendix*, Fig. S1*B*) animals. We also successfully reproduced the effects of protein kinase C (PKC)–neurogranin interactions on postsynaptic LTP in CA1 (16) (*SI Appendix*, Fig. S1*C*) and β-adrenergic receptor and stimulation frequency-dependent plasticity in V1 (17) (*SI Appendix*, Fig. S1*D*).

To compare the effects of SCZ for a range of plasticity protocols across brain regions, we used our unified model of

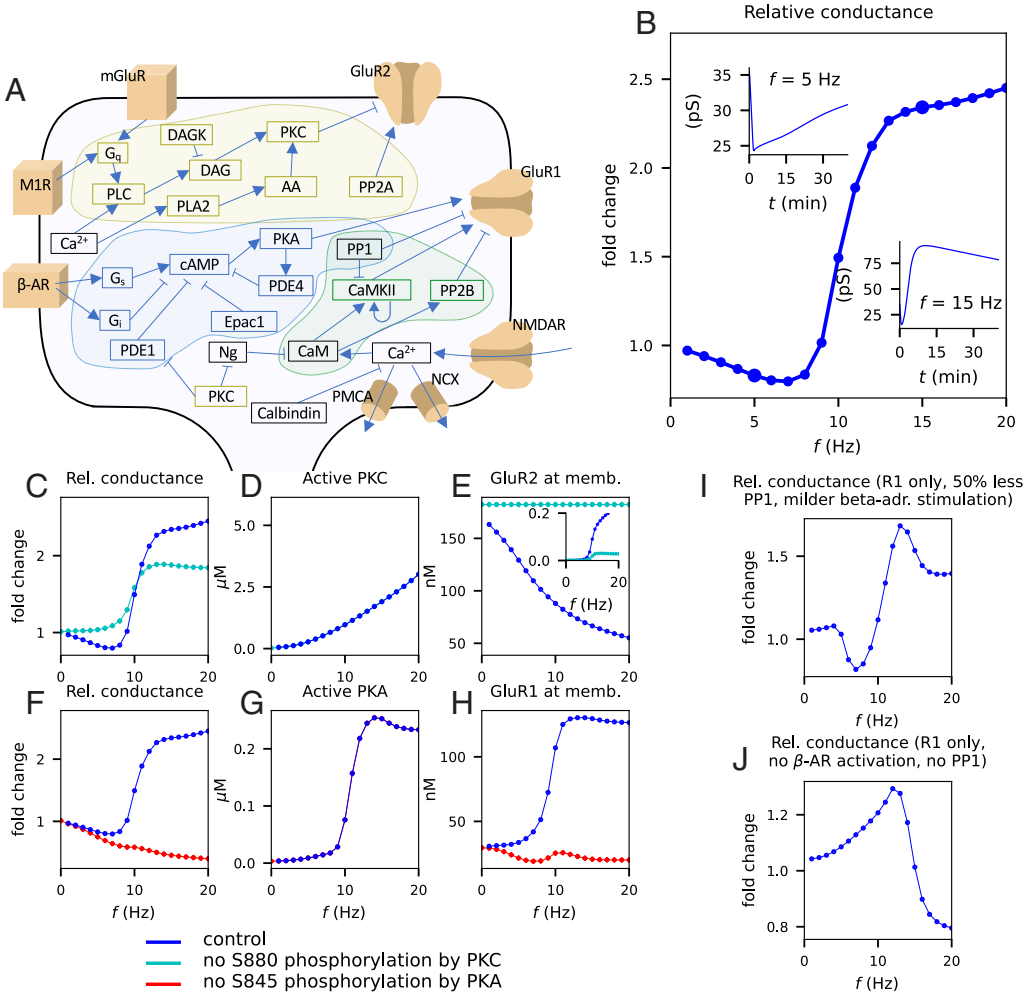

Fig. 1. The model predicts Bienenstock-Cooper-Munro (BCM)-like plasticity where low input frequencies induce LTD and high ones LTP. (*A*) Illustration of the cell membrane-level mechanisms and intracellular signaling pathways described by our model. (*B*) Relative synaptic conductance 30 min after stimulus onset as a function of input frequency, given a fixed stimulation time of T = 100 s. *Insets*: Time course of the synaptic conductance for input frequencies 5 Hz (*Left*) and 15 Hz (*Right*). (*C*) Relative synaptic conductance 30 min after stimulus onset in the control case (blue) and when phosphorylation of S880 of GluR2 by PKC was disabled (cyan). (*D*) Peak concentration of active PKC (all forms) during the simulation as a function of input frequency. (*E*) Concentration of membrane-inserted GluR2 subunits 30 min after stimulus onset in the control (blue) and S880-blocked (cyan) cases. *Inset*: Probability of membrane-inserted AMPAR tetramers being homomeric R1-type 30 min after stimulus onset according to our statistical rule (*SI Appendix*, equation 11; see ref. 11 for details). (*F*) Relative synaptic conductance 30 min after stimulus onset in the control case (blue) and when phosphorylation of S845 of GluR1 by PKA was disabled (red). (*G*) Peak concentration of catalytic subunit of PKA during the simulation as a function of input frequency. (*H*) Concentration of membrane-inserted GluR1 subunits 30 min after stimulus onset in the control (blue) and S845-blocked (red) cases. (*I*) Relative synaptic conductance in a PP1-reduced, GluR1-only synapse with milder β-adrenergic stimulation. This synapse produces bidirectional plasticity that is independent of the PKC-GluR2 pathway. (*J*) Relative synaptic conductance in a GluR1-only synapse without PP1 and without β-adrenergic stimulation. This synapse produces an inverse LTP/LTD curve. In the simulations of blocked S845 phosphorylation in panels (*E* and *G*), the loss of S845 activity was compensated by a spontaneous phosphorylation where the reaction rate of the added reaction was fitted so that the baseline synaptic conductance was equal to that in the default model.

postsynaptic plasticity with a standardized frequency-controlled stimulation protocol with which to study the effects of SCZ-associated genes on different types of plasticity. The stimulation protocol consisted of evenly spaced 3-ms Ca^{2+} input pulses for 100 s where we varied the frequency (and number) of the input pulses. We then measured the total synaptic conductance 30 min after the stimulus onset as a function of the stimulation frequency.

Using the default protein concentrations and a GluR1-to-GluR2 ratio of 1:3, our model produces a Bienenstock-Cooper-Munro (BCM) type plasticity curve, where low stimulation frequencies produced LTD and high stimulation frequencies produced LTP (Fig. 1*B*). The LTD was PKC dependent (Fig. 1*C*), mediated by GluR2 endocytosis (Fig. 1 *D* and *E*), while the LTP induced by high stimulation frequencies was PKA dependent (Fig. 1*F*) and was mediated by GluR1 exocytosis (Fig. 1 *G* and *H*). Moreover, the LTP induced by high stimulation frequencies was amplified by PKC (Fig. 1*C*) because the PKC-mediated GluR2 endocytosis increases the likelihood of α-amino-3-hydroxy-5-methyl-4-isoxazolepropionic acid receptor (AMPAR) tetramers being large-conductance homomeric AMPARs when the stimulus frequency is high (Fig. 1 *E*, *Inset*) (11).

The bidirectional plasticity of Fig. 1*B* relies on both GluR1 and GluR2 dynamics. However, purely GluR1-based bidirectional plasticity where the LTD was mediated by dephosphorylation of S845 has been observed in CA1 (18) and modeled in ref. 19. When we used a GluR1-only synapse (GluR1-to-GluR2 ratio of 1:0) and decreased the PP1 concentration by 50%, our model predicted a BCM-like plasticity curve (Fig. 1*I*). Our model also predicted that when PP1 was removed and the β-adrenergic receptor activation was blocked the GluR1-only synapse switched into an anti-BCM or anti-Hebbian mode of plasticity (Fig. 1*J*) occasionally observed in the cortex (20) or striatum (21).

Taken together, our model equipped with default protein concentrations produces a stereotypic bimodal, BCM-like plasticity. Next, we use this framework for assessing the effects of SCZ-associated genes on cortical synaptic plasticity.

Risk Genes Encoding Synaptic Intracellular Signaling Proteins Affect Cortical LTP/LTD. Impaired synaptic plasticity has been suggested as a unifying mechanism behind SCZ symptoms and pathogenesis (3, 22), but it remains unknown whether and how the implicated risk variants (9) can affect the induction of LTP/LTD. To identify the set of plasticity-related genes conferring a risk of SCZ, we used two sources: psychiatric GWAS data from the Psychiatric Genomics Consortium and expression data from the CommonMind Consortium (*SI Appendix*). We used our unified model of postsynaptic plasticity to identify which alterations of expression of the risk proteins modify which types of cortical postsynaptic plasticity. We implemented the effects of SCZ genetic alterations by altering the expression (both over- and underexpression) of the implicated proteins by ±20% and evaluated the plasticity curves in response to the standardized protocols described above.

The altered expression of the risk proteins identified by GWAS or expression data produced diverse effects on LTP/LTD in the cortex (Fig. 2). In the PKA pathway, overexpression of PP1 by 20% decreased the basal synaptic strength and amplified the LTP (Fig. 2*A*, red), and similar effects were obtained by underexpression of PKA (Fig. 2*B*, gray) and overexpression of PDE4 (Fig. 2*C*, red). These effects were mediated by altered S845-phosphorylation-driven membrane expression of GluR1 subunits (*SI Appendix*, Fig. S2 *A–C* and *G–I*). In the PKC pathway, overexpression of PLA2 amplified both LTD and LTP (Fig. 2*D*), similar to overexpression of PKC (*SI Appendix*, Fig. S2*M*). The effects of these parameter changes are attributed to their impact on S880-phosphorylation-mediated GluR2 endocytosis (*SI Appendix*, Fig. S2 *D*, *E*, *J*, and *K*). Altered expression of CaMKII by ±20% did not significantly alter the LTP/LTD amplitude (*SI Appendix*, Fig. S2*N*). By contrast, overexpression of neurogranin (Fig. 2*E*) or sodium-calcium exchanger (NCX) (Fig. 2*F*), both of which lead to an increased amount of input Ca^{2+} required to activate CaM, caused a rightward shift in the transition from LTD to LTP. Overexpression of NCX also decreased baseline I1 activity and, consequently, increased PP1 availability, which led to increased baseline GluR1 exocytosis (*SI Appendix*, Fig. S2*F*) and thus an increased baseline conductance (Fig. 2 *F*, *Inset*). Alterations of the expression of Gq (*SI Appendix*, Fig. S2*O*), mGluR (*SI Appendix*, Fig. S2*P*), calbindin (*SI Appendix*, Fig. S2*Q*), DAGK (*SI Appendix*, Fig. S2*R*), or Gi (*SI Appendix*, Fig. S2*S*) by ±20% had little or no effect. Decreased expression levels (gray) of the risk proteins always had qualitatively opposite effects than the increased levels (red; Fig. 2 *A–F* and *SI Appendix*, Fig. S2 *M–S*).

While the alterations in the gene-expression levels are likely to vary within SCZ patients due to the heterogenic disease phenotype and polygenic architecture, indications of the direction and magnitude of the altered expression can be obtained from post-mortem studies. We estimated the relative difference in the expression levels of the SCZ-associated genes of *SI Appendix*, Table S1*A* between SCZ patients and HCs in PFC and ACC using the CommonMind data. We repeated the simulations of Fig. 2 *A–F* and *SI Appendix*, Fig. S2 *M–S* with these expression-level factors, either all combined (Fig. 2*G*) or a single protein-concentration change at a time (*SI Appendix*, Fig. S3 *A–K*). When all expression alterations were combined, both PFC- and ACC-like alterations affected the baseline synaptic strength and the LTP magnitude, but the effects of the variants corresponding to expression data from PFC were milder (LTP amplitude decreased by 1.9%) than the effects of those from ACC (LTP amplitude decreased by 7.7%; Fig. 2*G*). The predicted alterations of LTP magnitude in the PFC were mostly driven by altered PKA expression, whereas those in the ACC were mostly driven by altered expression of PKA, PP1, and PLA2 (*SI Appendix*, Fig. S3 *A–C*): these alterations caused the LTP amplitude to be decreased by 1.2% (PKA alteration in ACC, *SI Appendix*, Fig. S3*A*), 3.3% (PP1 alteration in ACC, *SI Appendix*, Fig. S3*B*), 2.3% (PLA2 alteration in ACC *SI Appendix*, Fig. S3*C*), or 1.5% (PKA alteration in PFC, *SI Appendix*, Fig. S3*A*) while alterations of other risk proteins affected the LTP amplitude by a maximum of ±0.8% (*SI Appendix*, Fig. S3 *D–K*). Both PKA- and PKC-dependent pathways of our model seem to be instrumental in mediating these effects since removal of these pathways decreased the predicted impact of the ACC- and PFC-like alterations (*SI Appendix*, Fig. S4).

To confirm our finding of impaired LTP, we simulated the plasticity outcome using a personalized approach, where the initial concentrations of proteins of *SI Appendix*, Table S1*A* were determined in a subject-wise manner based on the CommonMind expression data (Fig. 2 *H* and *I*). The amplitude of the plasticity was significantly (U test, $P < 0.05$) decreased in the SCZ group for the LTP induced by 12, 14, 16, 18, and 20 Hz stimulation in the simulations based on ACC expression data ($P = 0.00034$, $3.1 \cdot 10^{-5}$, $2.4 \cdot 10^{-5}$, 0.00018, and 0.00064 for 12, 14, 16, 18, and 20 Hz, respectively), but only the decreases in LTP induced by 12 and 14 Hz stimulation were significant ($P = 0.0029$ and $P = 0.016$ for 12 and 14 Hz, whereas $P =$ 0.67, 0.84, and 0.95 for 16, 18, and 20 Hz, respectively) in the

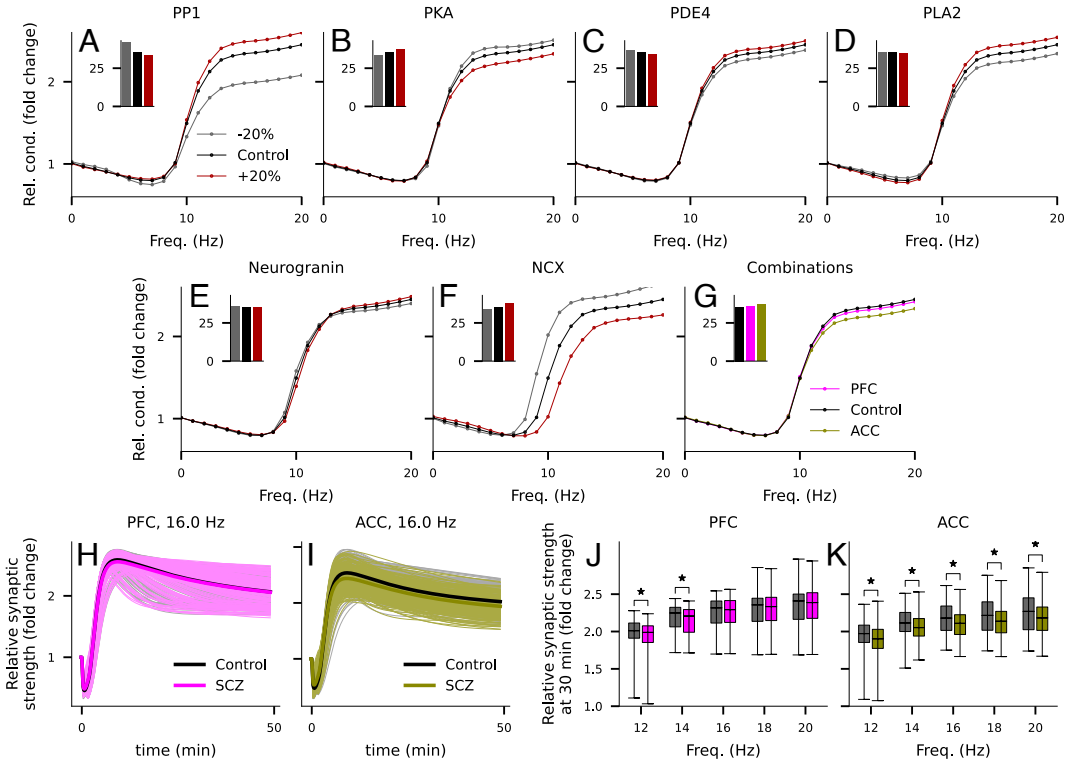

Fig. 2. Altered expression of synaptic proteins associated with the risk of SCZ can impair or enhance LTP/LTD. (*A*–*F*) The experiment of Fig. 1*B* was repeated with altered expression of the risk proteins of *SI Appendix*, Table S1*A*, namely PP1 (*A*), PKA (*B*), PDE4 (*C*), PLA2 (*D*), neurogranin (*E*), and NCX (*F*). Red and gray curves represent the data from simulations where the underlying protein concentration was 20% higher (red) or lower (gray) than in the default model (black). The x and y axes show the frequency of inputs and the relative synaptic conductance 30 min after stimulus onset, respectively. *Insets*: the baseline synaptic conductance (pS). (*G*) The experiment of Fig. 1*B* was repeated with a combination of expression-level alterations of the 10 genes affecting 9 model parameters (for PFC, pink) or the 12 genes affecting 9 model parameters (for ACC, green; see *SI Appendix*, Table S1*A*) as suggested by postmortem data. (*H* and *I*) The experiments of Fig. 2*G* were repeated using subject-wise expression patterns for the underlying genes. The plots show the time courses of the relative synaptic conductance in response to 16 Hz stimulation for 100 s. The dim gray curves represent the subject-wise simulation results for HC subjects (N = 215 in PFC and N = 251 in ACC) and the dim pink (PFC; N = 211) and light green (ACC; N = 227) curves represent those for SCZ subjects. The thick curves represent the averages over the diagnostic groups. (*J* and *K*) Box plots of the predicted post-30 min synapse weights for stimulation frequencies 12 to 20 Hz in the subject-wise simulations. The asterisks denote statistically significant differences between the diagnostic groups (*U* test, $P < 0.05$).

simulations based on the PFC expression data (Fig. 2 *J* and *K*). We also confirmed the robustness of this result by simulating the plasticity in synapses where the expression of the risk genes was altered using alternative strategies for determining the parameter changes based on the CommonMind data. A majority of these strategies yielded similar results, namely, that the gene-expression profiles of SCZ subjects compared to HCs in postmortem ACC predicted an impaired LTP amplitude (*SI Appendix*, Fig. S5).

Taken together, our simulations show that mild changes in expression levels of proteins associated with the risk of SCZ can weaken or strengthen the cortical LTP/LTD, and that the expression-level alterations observed post mortem in ACC of SCZ patients can cause a significant decrease in LTP amplitude.

Risk Genes Encoding Both Voltage-Gated Ion Channels and Intracellular Signaling Proteins Regulate Cortical STDP. Apart from the stimulation frequency-dependent plasticity protocols, STDP is a protocol widely used for studying plasticity in the cortex and hypothesized to be a generic cellular-level learning rule in the brain (23). In STDP, both pre- and postsynaptic neurons are stimulated by current injection (or extracellular stimulation) to produce release of neurotransmitter on the presynaptic side and an action potential on the postsynaptic side. The outcome of the plasticity critically depends on the timing between pre- and postsynaptic stimuli (23). STDP is thus dependent on the membrane excitability properties of the postsynaptic neuron. We have previously studied the effects of SCZ-associated ion channel-encoding genes on pyramidal cell excitability (24–26) using biophysically detailed neuron models, and the same framework can be used to investigate how the integration of STDP-inducing pre- and postsynaptic stimuli is affected by these genes. Here, we test the effects of alterations of ion-channel expression in the postsynaptic neuron on STDP and how they compare to the modifications to the STDP curve caused by altered expression of intracellular signaling proteins.

For this multiscale investigation, we used 1) the biophysically detailed model for layer II/III pyramidal cell (27) (L23PC) for determining the size and time course of N-methyl-D-aspartate receptor (NMDAR)-mediated Ca^{2+} inputs for each pre/postsynaptic pairing interval (Fig. 3*A*) and 2) our biochemically detailed model of signaling pathways mediating plasticity in response to Ca^{2+} and neuromodulatory inputs (*SI Appendix*). We altered the maximal ion-channel conductances of the risk proteins in the pyramidal cell model as suggested by the genetic analysis (*SI Appendix*, Table S1*B*). We also evaluated the interaction between altered expression of ion channel-encoding and plasticity-regulating proteins.

First, we validated our updated model by replicating the experimentally observed neuromodulator-gated STDP curve for layer IV→II/III pyramidal cell synapses in the visual cortex. Similar to experimental data (28) and our previous model (11), little or no plasticity is observed in the absence of

neuromodulators (Fig. 3*B*, blue), LTP is obtained when the pairing stimuli are administered with β-adrenergic input (Fig. 3*B*, brown), LTD is obtained when the stimuli are administered with cholinergic input (Fig. 3*C*, purple), and pairing-interval-dependent LTP/LTD is obtained when both neuromodulators are present (Fig. 3*C*, black). Next, we simulated the effects of altered expression of ion channels in the postsynaptic neuron on the cortical STDP (Fig. 3 *D* and *E* and *SI Appendix*, Fig. S6 *A–E*). Overexpression of CACNA1C (Fig. 3*D*, red) and KCNQ3 (*SI Appendix*, Fig. S6*A*) led to decreased LTP amplitudes—a mild decrease of LTP amplitude was also observed for increased leak channel conductance (a putative effect of overexpression of KCNK4; *SI Appendix*, Fig. S6*B*). By contrast, overexpression of HCN1 mildly strengthened LTP (Fig. 3*E*). The increase of LTP amplitude by increase of hyperpolarization-activated cyclic nucleotide-gated (HCN) channels is explained by a generally increased dendritic excitability (29), while the LTP-impairing effect of increased high-voltage activated (HVA) Ca^{2+} conductance was caused by increased SK activity (25). Altered expression of SCN1B or SCN9A (*SI Appendix*, Fig. S6*C*), KCNB1 or KCND3 (*SI Appendix*, Fig. S6*D*), and CACNA1I (*SI Appendix*, Fig. S6*E*) had little effect on STDP. The effects of the

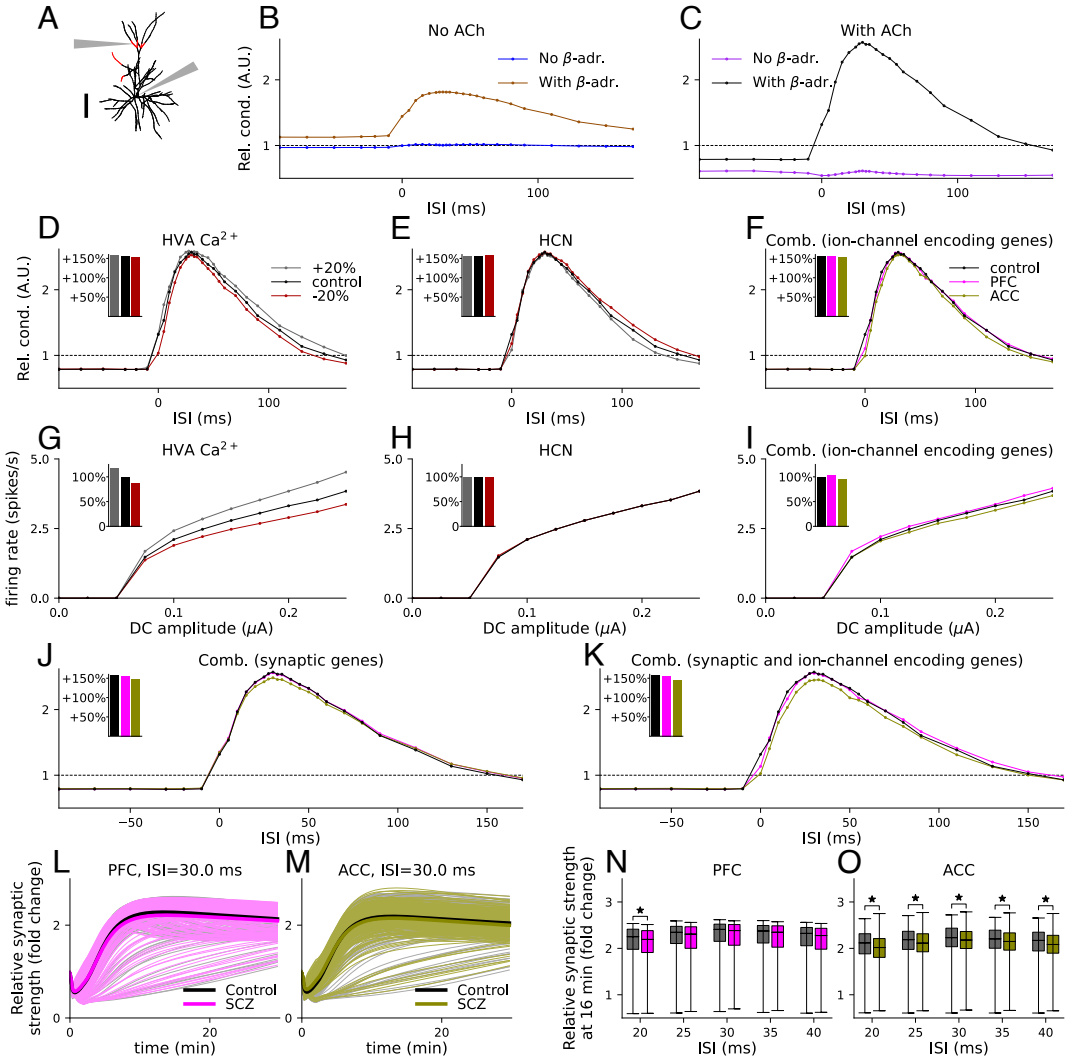

Fig. 3. Altered expression of SCZ risk genes encoding voltage-gated ion channels or synaptic proteins of the postsynaptic neuron can affect STDP. (*A*) Illustration of the L23PC model used for determining the Ca^{2+} time course. Compartments where the postsynaptic spine can be inserted are highlighted in red. The *Top* arrow represents an exemplary location of the postsynaptic spine and the *Bottom* arrow points at the soma where the burst of square pulse currents is injected. (Scale bar, 100 μm.) (*B* and *C*) Our model reproduces neuromodulator-gated STDP reported in ref. 28. The curves show the relative synaptic strength in response to 120 stimuli 16 min after stimulus onset as a function of interstimulus interval (negative values of ISI correspond to post–pre stimulus protocols) in the absence of cholinergic and β-adrenergic neuromodulation (*B*, blue), in the absence of cholinergic but presence of β-adrenergic neuromodulation (*B*, brown), in the absence β-adrenergic but presence of cholinergic neuromodulation (*C*, purple), and in the presence of both neuromodulators (*C*, black). (*D* and *E*) The STDP curve when the postsynaptic neuron expresses 20% more (red) or less (gray) voltage-gated ion channels, namely, high-voltage-activated Ca^{2+} channels (*D*) or I_h channels (*E*). *Insets*: maximal LTP value of the curve. (*F*) The STDP curve with the PFC- (pink) and ACC-like (green) combinations of variants of ion-channel encoding genes. (*G–I*) The (f–i) curves, i.e., spiking frequency of the postsynaptic neuron as a function of the amplitude of DC applied to soma, corresponding to the variants of panels (*D–F*). *Insets*: The firing rate in response to DC of amplitude 0.25 μA, normalized by the response of the default neuron model (black). (*J*) The STDP curve for the combinations of variants of synaptic risk genes as in Fig. 2*G*. (*K*) The STDP curve for the combinations of synaptic protein-affecting variants of panel (*J*) and ion-channel-affecting variants of panel (*F*). (*L* and *M*) The time course of the relative synaptic strength in subject-wise simulations of LTP induction in response to pre–post stimuli with 30 ms interval. The dim gray curves represent the subject-wise simulation results for HC subjects and the dim pink (PFC; *L*) and green (ACC; *M*) curves represent those for SCZ subjects. The thick curves represent the averages over the diagnostic groups. (*N* and *O*) Box plots of the predicted post-15 min synapse weights in PFC (*N*) and ACC (*O*) in the subject-wise simulations of pre–post intervals 20 to 40 ms. The asterisks denote statistically significant differences between the diagnostic groups (*U* test, $P < 0.05$).

altered expression of ion channels on post–pre LTD were small (Fig. 3 *D* and *E* and *SI Appendix*, Fig. S6 *A–E*). We also analyzed the effects of these variants on neuron excitability by measuring the predicted f-I curves, namely, firing frequencies in response to DC of different amplitudes. The maximal LTP amplitudes of the ±20% variants were correlated (Pearson correlation coefficient 0.71, *P*-value = 0.0041) with the firing frequencies in response to somatic DC, indicating that the increase in LTP was driven by a generic increase in the single-cell excitability (Fig. 3 *G* and *H* and *SI Appendix*, Fig. S6 *F–J*). Exceptions to this pattern were the SCN1B or SCN9A-encoded fast Na^+ channel, where overexpression had little effect on LTP response but increased the firing response (*SI Appendix*, Fig. S6 *C* and *H*), and HCN and M-type channels where altered expression affected the STDP but had little or no effect on somatically induced firing of action potentials (Fig. 3 *E* and *H* and *SI Appendix*, Fig. S6 *A* and *F*).

Simulations with combinations of altered expression levels of these voltage-gated ion channels as measured in PFC and ACC showed that LTP amplitude may be reduced (Fig. 3*F*) and intrinsic pyramidal cell excitability altered (Fig. 3*I*) in PFC and ACC in SCZ patients. The effects on LTP amplitude were, however, mild (maximal LTP amplitude +156% and +154% in PFC- and ACC-like alterations, respectively, compared to +157% in control; Fig. 3*F*) suggesting that the changes in STDP caused by expression-level alterations of different ion channels can compensate for each other. The effects on intrinsic pyramidal cell excitability were different for PFC-like alterations compared to ACC-like alterations (firing frequency increased by 2.7% and decreased by 4.1% for PFC- and ACC-like alterations, respectively; Fig. 3*I*).

We asked how the alterations in ion channel-encoding and plasticity-regulating genes interact to affect the STDP. We first simulated the effects of altered expression of intracellular signaling proteins (Fig. 3*J*). The effect of PFC-like alterations was smaller (maximal LTP amplitude +156% compared to +157% in control) than those of ACC-like alterations (maximal LTP amplitude +148%; Fig. 3 *J*, *Inset*). When the combination of the ion-channel variants was used together with the combination of synaptic gene variants, the LTP amplitude was more strongly decreased, particularly in a synapse expressing ACC-like alterations (maximal LTP amplitude +155% and +145% in PFC- and ACC-like alterations, respectively, compared to +157% in control; Fig. 3*K*). We confirmed the significance of the effects of the ACC-like alterations by performing subject-wise simulations (Fig. 3 *L* and *M*). The amplitude of the LTP induced by pre–post pairs of stimulus (inter-stimulus interval (ISI) = 20, 25, 30, 35, 40 ms) stimuli was significantly smaller (*U* test, $P < 0.05$) in the SCZ subjects than in the HCs according to the ACC postmortem expression data ($P = 0.0026$, 0.018, 0.045, 0.038, 0.021 for ISI = 20, 25, 30, 35, and 40 ms, respectively; Fig. 3*O*), but the corresponding difference in simulations based on PFC expression data was only significant for 20 ms ISI ($P = 0.035$, 0.093, 0.23, 0.16, and 0.11 for ISI = 20, 25, 30, 35, and 40 ms; Fig. 3*N*).

Taken together, our results suggest that altered expression of ion-channel encoding SCZ-associated genes can alter the LTP amplitude in the STDP protocol, and simulations using postmortem expression data, especially those from ACC, support a decrease in pre–post stimulus-induced LTP amplitude.

Plasticity in Response to Stimuli Used in the Clinical Phenotype of VEP Modulation May Be Altered by SCZ-Associated Gene Variants. SCZ has been linked to synaptic abnormalities both by genetics analyses and postmortem studies, but mechanistic links mapping these deviances to disorder symptoms and phenotypes are missing (30). A promising phenotype for study is VEP, the plasticity of which is reported to be impaired in psychotic disorder patients (13, 31). The VEP is a visual stimulus-related EEG response and plasticity or modulation of VEP is the potentiation of VEP amplitudes after long-lasting continuous checkerboard reversal stimulation (32). Although the LTP-like plasticity of VEP is likely to reflect synaptic plasticity occurring in multiple parts of VEP-related brain circuitry, it shares properties with traditional monosynaptic LTP, such as NMDAR dependency (31, 33, 34). Here, we explored the cortical synaptic plasticity caused by stimuli simulating the VEP-plasticity protocol and tested the effects of SCZ-associated genes on this form of plasticity.

To model the synaptic inputs in the VEP protocol, we stimulated the synapse with an action potential every 500 ms to mimic a checkerboard reversal with a frequency of 2 reversals/s for 10 min (35), and measured the effects on synaptic conductance 10 to 60 min after the stimulus onset. Each synaptic input was modeled as a square pulse influx of Ca^{2+} lasting for 3 ms, which was by default accompanied by a flux of β-adrenergic agonist (5 particles/ms for 3 ms) as well as glutamate and cholinergic ligands (10 particles/ms for 3 ms) into the vicinity of the synapse, as in the experiments of Figs. 1 and 2. We tested the LTP/LTD response of the synapse to these stimuli using two extreme GluR1:GluR2 ratios, namely, 1:0 (GluR1-type) and 0:1 (GluR2-type).

Our model predicted that both GluR1-type (LTP; Fig. 4 *A* and *B*) and GluR2-type (LTD; Fig. 4 *C* and *D*) synapses underwent plasticity that was maintained for more than 1 h. Neuromodulators were critical, as in the absence of neuromodulators the VEP protocol did not induce long-lasting plasticity changes (Fig. 4 *A* and *C*). A qualitatively similar response to an alternative stimulation protocol, namely, 8.8 Hz stimulation for 2 min as used in ref. 13, was obtained (*SI Appendix*, Fig. S7 *A* and *B*).

Similar to the plasticity induced by the standard protocol, VEP protocol-induced plasticity was affected by alterations in PP1 (Fig. 4*E*), PKA (Fig. 4*F*), and PDE4 (Fig. 4*G*) in GluR1-type synapses, though not in GluR2-type synapses. In contrast, alterations of PLA2 (Fig. 4*H*) and PKC (*SI Appendix*, Fig. S7*C*) affected the plasticity in a GluR2-type synapse but not GluR1-type synapse. Neurogranin and NCX affected the plasticity of both types of synapses (Fig. 4 *I* and *J*). No other risk proteins (including CaMKII) modified plasticity in response to the VEP-like stimulus when quantity was changed by ±20% (*SI Appendix*, Fig. S7 *D–I*). PFC-like alterations of expression levels only mildly reduced the plasticity in a GluR1-type synapse (the increase in synaptic strength at 60 min was +108% compared to +114% in control) but not the GluR2-type synapse (Fig. 4*K*, pink). By contrast, ACC-like alterations strongly reduced the VEP-stimulus-induced plasticity in the GluR1-type synapse (in a GluR1-type synapse, the increase in synaptic strength was +93% compared to +114% in control) but not the GluR2-type synapse (Fig. 4*K*, green). The effects of the variant combinations on the plasticity in the GluR1-type synapse were driven by modifications of PKA-pathway genes: the impacts of the variant combinations were nearly abolished in a GluR1-type synapse when the PKA-pathway-affecting genes were excluded from the combination (*SI Appendix*, Fig. S7 *J–O*).

We confirmed the significance of these findings with the simulations based on subject-wise expression data. In subject-wise simulations of the VEP-like stimulation of a GluR1 synapse, both PFC- and ACC-like expression alterations caused a significant

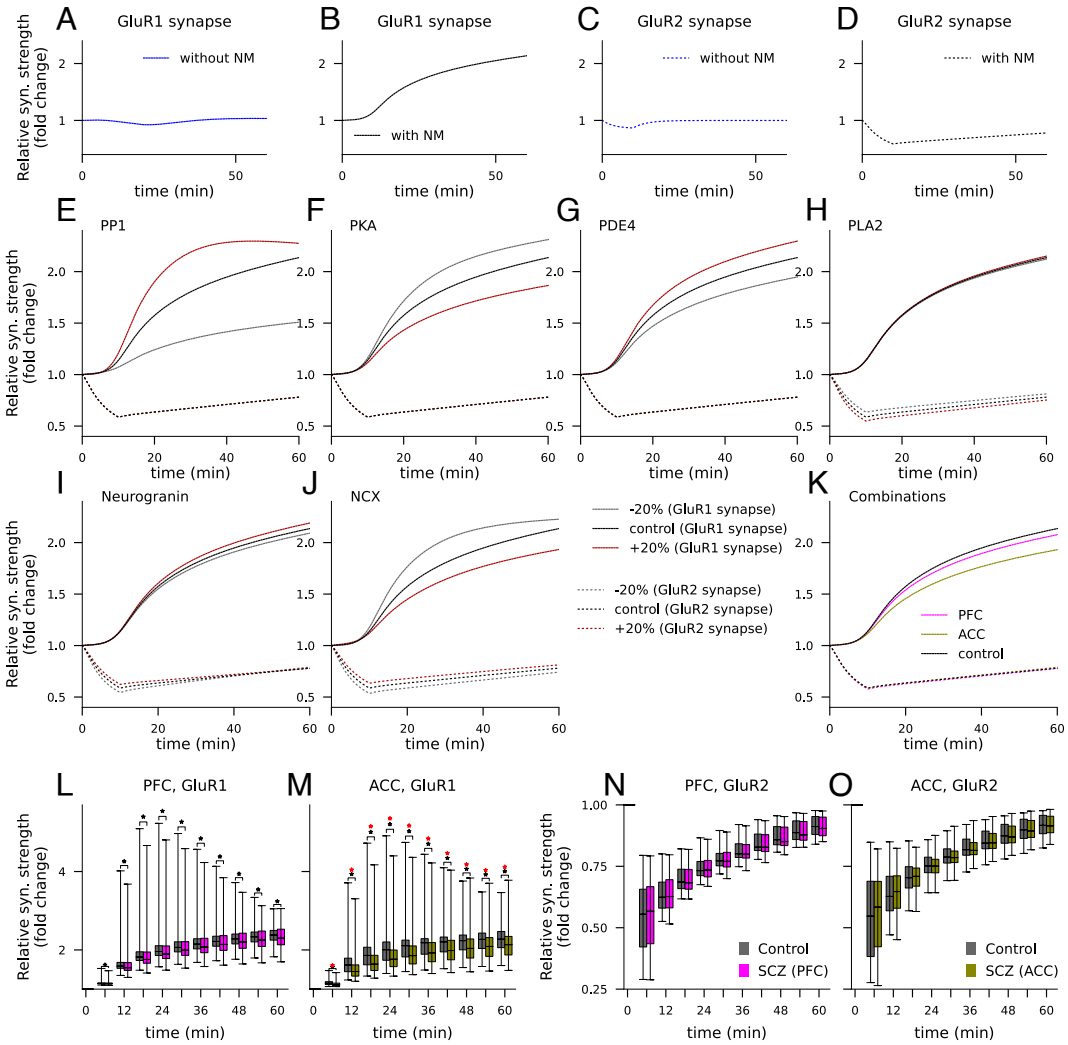

Fig. 4. Altered expression of risk genes encoding synaptic proteins alters the plasticity response to VEP-like stimulus protocols. (*A*–*D*) Time course of relative synaptic conductance in response to VEP-like stimulus (1,200 stimuli administered during the 0 to 10 min interval) in the absence (*A* and *C*; blue) or presence (*B* and *D*; black) of neuromodulators in a synapse where all GluRs were GluR1 (*A* and *B*; solid) or GluR2 (*C* and *D*; dashed) type. (*E*–*J*) Time course of the synaptic conductance in the VEP protocol with neuromodulatory stimulation in GluR1 (solid) or GluR2-type (dashed) synapses when the expression of SCZ risk protein PP1 (*E*), PKA (*F*), PDE4 (*G*), PLA2 (*H*), neurogranin (*I*), or NCX (*J*) was altered. (*K*) Time course of the synaptic conductance for a combination of PFC-like (pink) and ACC-like (green) variants. (*L*–*O*) The experiments of panel (*K*) were repeated using subject-wise expression patterns. The box plots show the relative synaptic conductance in response to VEP-like stimulus in a GluR1-type (*L* and *M*) or GluR2-type (*N* and *O*) synapse. Data for 6 to 60 min after stimulus onset are shown for both control (gray) and SCZ (pink, green) population for PFC- (*L* and *N*) and ACC-based (*M* and *O*) simulations. The black asterisks denote statistically significant differences between the diagnostic groups (*U* test, $P < 0.05$), and the red asterisks denote differences that were significant using a stricter threshold ($P < 0.005$).

decrease in the LTP amplitude for each considered time point (6 to 60 min after stimulus onset in 6-min intervals; *U* test, $P < 0.05$), but only the effects of the ACC-like expression alterations were significant when a smaller *P*-value threshold (*U* test, $P < 0.005$) was used (Fig. 4 *L* and *M*). Consistent with the experiments based on group-averaged expression data, the differences between SCZ and HC in plasticity responses in the GluR2-type synapse were nonsignificant (Fig. 4 *N* and *O*).

Taken together, our results suggest that the modulation of synaptic strength by a VEP-like stimulus protocol can be moderately altered by risk proteins of SCZ. When the expression of the risk proteins is altered to reflect the expression alterations observed post mortem in SCZ, the PKA-pathway-dependent potentiation of GluR1-containing synapses by the VEP-like stimulus protocol is weakened. Our results shed light on the polygenic mechanisms of VEP modulation deficits in SCZ and may pinpoint a generic vulnerability of plasticity in the mental disorder.

Genotypes and Electrophysiological Data Support the Contribution of SCZ-Associated Plasticity-Regulating Genes to the Deficit of LTP-Like Plasticity of the VEP. Although our model predictions for effects of altered expression of SCZ on generic LTP/LTD are difficult to validate, our predictions for the effects on plasticity induced by VEP protocol can be compared to EEG data collected from corresponding experiments. Here, we tested whether our model predictions align with genetic associations found in the genotype–phenotype data. For this, we used a large dataset from The Thematically Organized Psychosis (TOP) Study (36) containing genetic and EEG data of VEP modulation from 286 HCs (37, 38). We calculated PRSs based on SNPs in different plasticity-regulating or ion channel-encoding genes (*SI Appendix, Materials and Methods* and Table S2) for each subject and determined their association with the EEG phenotypes by fitting a linear model, where the EEG index was regressed against the considered PRS, age, and sex. We only included SNPs that were indicative of SCZ risk (*P*-value $< 10^{-5}$) in the recent

GWAS (8). We quantified the associations using the Pearson correlation coefficient, the β coefficient, and the P-value for the PRS obtained from the linear model.

Of the VEP indices measured 2 to 4 min after the end of the continuous 10 min stimulation, the modulation of C1 (Fig. 5*A*) and N1b (Fig. 5*C*) amplitude were not significantly associated with the PRSs that we considered, whereas the P1 modulation (Fig. 5*B*) was significantly associated with the following PRSs: 1) the PRS based on SNPs in the genes encoding ion channels and plasticity-related proteins of *SI Appendix*, Table S2 ($\beta = -141$, correlation coefficient -0.12, $P = 0.039$), 2) the PRS based on SNPs in a subset of plasticity-regulating genes affecting plasticity via the PKA pathway (purple genes of *SI Appendix*, Table S2; $\beta = -68$, correlation coefficient -0.13, $P = 0.029$), and 3) the PRS based on SNPs in ion-channel encoding genes (light green genes of *SI Appendix*, Table S2; $\beta = -89$, correlation coefficient -0.14, $P = 0.020$). We did not observe a significant association with the PRS based on SNPs in the plasticity-regulating genes of *SI Appendix*, Table S2 ($\beta = -82$, correlation coefficient -0.08, $P = 0.158$) or with the PRS based on SNPs of the genes of *SI Appendix*, Table S1 ($\beta = -47$, correlation coefficient -0.10, $P = 0.119$). Fig. 5 *D*–*I* shows the values of P1 modulation plotted against the tested PRS values. Apart from the PRS based on PKC-pathway genes (Fig. 5*G*; $\beta = 35$, correlation coefficient 0.07, $P = 0.266$), all these β coefficients were negative, indicating that the presence of SCZ-risk SNPs in these sets of genes was predictive of lower postmodulation P1 amplitude in the VEP experiment and thus suggestive of impaired LTP-like plasticity. These results held also for PRSs calculated from the same sets of genes using alternative thresholds ($5{\cdot}10^{-6}$ and 10^{-6}) for the inclusion of the SNPs (*SI Appendix*, Fig. S8 *A* and *B*). We went on to confirm the relevance of the SNPs in synapse-specific genes by using an alternative set of genes, as introduced in ref. 39. Namely, we constructed a PRS based on the SNPs within the genes in the following categories (Table S4 of ref. 39): Intracellular Signal Transduction, Excitability, GPCR signaling, Protein cluster, Neurotransmitter metabolism, LGIC signaling, Ion balance/transport, and G-protein relay, totaling 432 genes. The modulation of P1 was significantly associated with this alternative synapse-specific PRS ($\beta = -102$, $P = 0.016$; *SI Appendix*, Fig. S8*C*).

Taken together, our analysis suggests that the modulation of VEP-P1 is influenced by variants within plasticity-regulating and ion channel-encoding risk genes of SCZ. The directions of the associations suggest that the presence of SCZ risk SNPs in ion-channels-encoding or PKA-coupled genes regulating plasticity decreases the LTP-like plasticity of VEP-P1.

Discussion

In this work, we analyzed the effects of SCZ-associated genes involved in synaptic plasticity on the amplitude and sensitivity of cortical LTP and LTD. We showed that mild alterations of expression levels of the proteins encoded by these genes can lead to significant alterations of threshold between LTD and LTP as well as LTP amplitude (Fig. 2), STDP amplitude (Fig. 3), and the plasticity induced by protocols for LTP-like plasticity of the VEP (Fig. 4). When we implemented the alterations of synaptic gene expression as observed in comparative postmortem experiments,

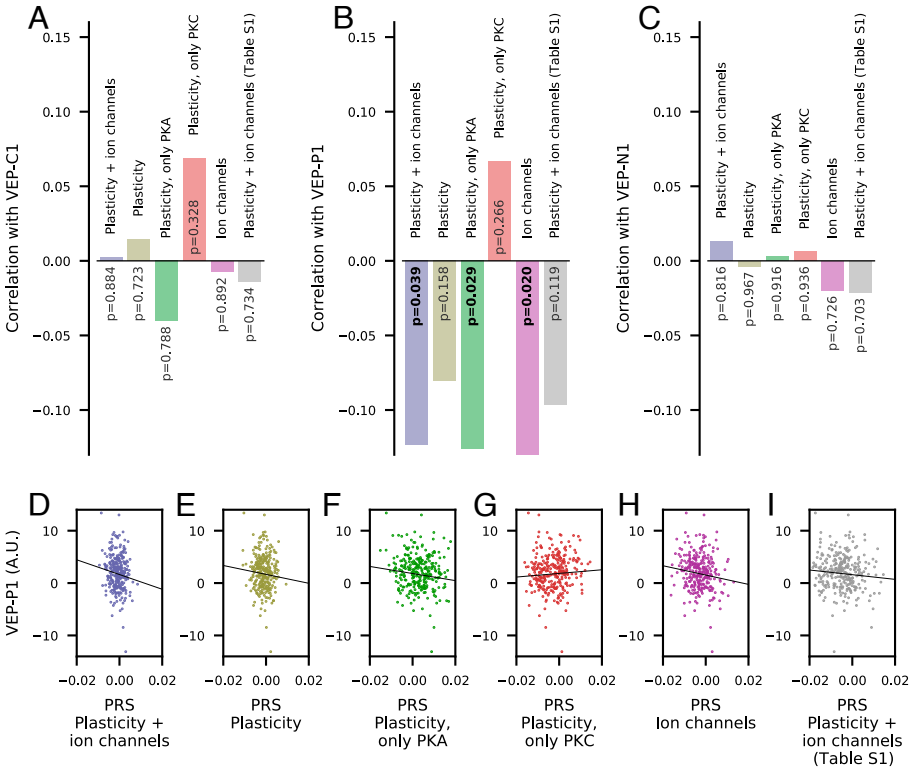

Fig. 5. Analysis of a genotyped EEG dataset of VEP modulation provides support for the involvement of SCZ-associated variants of genes regulating synaptic plasticity and genes encoding ion-channel subunits in impairment of cortical plasticity. (*A*–*C*) Pearson correlation coefficients between the modulation of the C1 amplitude (*A*), P1 amplitude (*B*), or N1b amplitude (*C*) and the six PRSs. The modulation of the VEP amplitudes C1, P1, and N1b is defined as the baseline amplitude of C1, P1, or N1b subtracted from the respective amplitude in the postmodulation blocks 2 to 4 min after the continuous 10 min stimulation. (*D*–*I*) P1 amplitude plotted against the six PRSs based on SNPs in the following gene sets: all genes of *SI Appendix*, Table S2 (*D*), genes encoding plasticity-related proteins (*E*), genes encoding plasticity-related proteins that primarily couple to PKA (*F*) or PKC (*G*) pathway, genes encoding ion channels or their subunits (*H*), or the genes implicated by GWAS or CommonMind data that were used to inform our model (*SI Appendix*, Table S1; *I*). The lines represent the effect of the PRS on the EEG index as obtained from the linear regression.

where gene expression in PFC and ACC were measured from SCZ patients and HCs, our model predicted a mild decrease in LTP amplitude for the PFC-like variant and a stronger decrease for the ACC-like variant (Fig. 2*G*). Similarly, both the PFC-like and ACC-like variants were predicted to reduce the amplitude of VEP-like plasticity, the ACC-like variant more than the PFC-like variant (Fig. 4*N*). The association of the genotype with the EEG response to VEP-like plasticity protocol (Fig. 5) supports our findings of impaired neocortical plasticity in SCZ.

There are at least five different kinds of indirect experimental evidence of altered synaptic plasticity in SCZ (cf. 22). Postmortem studies have reported 1) altered expression of synapse-associated genes (40) and 2) aberrant spine morphology (41) or spine density (42) in SCZ patients compared to HCs, the former observation being a likely culprit for altered synaptic plasticity in SCZ and the latter being its consequence. 3) Recent GWASes of SCZ have implicated a disproportionally large set of the genes that are associated with synaptic plasticity (8, 9). Furthermore, 4) certain phenotypes and endophenotypes of SCZ, such as altered modulation of LTP-like plasticity of the VEP (13), impaired mismatch negativity (43), and altered habituation of acoustic startle (44), together with 5) cognitive symptoms of SCZ such as impaired working memory (45) suggest that the very mechanisms of synaptic plasticity may be affected in the mental disease. Three of these modalities converge in this work. We selected the parameters to alter based on GWAS results (3), determined the magnitude of the parameter changes based on postmortem expression studies (1), and predicted the effects on phenotypic measures (4) using stimulation protocols designed to mimic the synaptic inputs expected to occur in the experiments of these phenotypes. Furthermore, since many genetic manipulations that impair plasticity also impair working memory in animals (46, 47), our results showing a decreased LTP amplitude may also prove relevant for deciphering the cause of cognitive dysfunction (5) in SCZ. The impairments of plasticity are likely to interact with alterations in the density and shape of certain types of neurons (48) as well as those in synthesis or conversion of neurotransmitters (49, 50), but exploring this requires network-level models and is out of the scope of the present work.

SCZ is a complex disorder with a polygenic architecture where individual common risk variants have a small effect (51). A cumulative effect of variants affecting the same biological process, such as neurotransmission and plasticity (9), is believed to be needed for disease development. Alternatively, some variants may lead to a certain subtype of SCZ and others to another subtype since the intrinsic heterogeneity is large in SCZ. While our theoretical analysis (±20% change in expression, Fig. 2 *A*–*F*) revealed different modes in which gene variants may alter the LTP and LTD, thus suggesting a potential for molecularly and functionally different alterations of plasticity, our CommonMind data-based simulations more clearly indicated the cumulative role of expression-level changes of the most central proteins in decreasing the total amplitude of plasticity (Fig. 2*G*, *SI Appendix*, Fig. S3 *A*–*C*).

It should be noted that there is incomplete evidence on altered expression of GWAS-identified risk genes in SCZ, an assumption that our approach is partly based on. For example, *SI Appendix*, Table S1 shows that while half of the considered ion channel-encoding GWAS-identified genes (CACNA1C, CACNA1D, and HCN1) reached the significance threshold in the expression data, none of the plasticity-regulating GWAS-identified genes did. Alternatives for this assumption are that the risk SNPs mediate the risk 1) by altering the transcription of other genes or 2) by direct effects on the structure of the encoded proteins. While usually only ultra-rare SCZ-associated variants are coding variants (i.e., result in proteins with mutated structure) (52), the hypothesis that many SCZ-associated SNPs only regulate gene transcription of genes other than themselves cannot be discarded either for common or rare variants. In fact, since the association of VEP modulation with the PRS based on the genes included in our modeling framework (*SI Appendix*, Table S1) was nonsignificant while the association with the PRS based on larger sets of plasticity-regulating genes was significant (Fig. 5), the RNA expression of the genes of *SI Appendix*, Table S1 may be affected by a larger number of SNPs in plasticity-regulating genes than those located in these genes alone—on the other hand, this can also mean that prediction of stronger differences between SCZ and HC could be obtained by our model if expression of additional plasticity-regulating genes were considered. Common SCZ-associated SNPs have also been shown to alter gene methylation (53, 54), and some variants are located in expression quantitative trait loci (55). Nevertheless, previous data do show that many GWAS-identified SCZ risk genes that have risk SNPs within their intragene region, e.g., CACNA1C, PDE4B, and NRGN (*SI Appendix*, Table S1), are themselves differentially expressed in SCZ (56–58).

Our genotype–phenotype data analysis was carried out in HCs. The sample we used was large (N = 286) compared to many other psychiatric EEG studies but not compared to genetic association studies, and thus our genotype–phenotype analyses should be replicated and further dissected in larger samples when they become available. Focusing exclusively on HCs helps to avoid the association being caused by a secondary factor, such as antipsychotics (59), but it may also further stress the contribution of common rather than rare variants to the studied phenotype and the suggested molecular pathways.

In this work, we specifically focused on a phenotype often encountered in SCZ patients and strongly suggestive of impairment of plasticity, namely, the deficit in the modulation of VEP (13). The animal-model correlate of this phenotype, the stimulus-specific response potentiation (SRP), has been found to be NMDAR dependent (60), making it likely to rely at least partly on postsynaptic plasticity. The SRP has been found obstructed by infusion of Myr-SIYRRGARRWRKL-OH (Myr-Zip) (61), a peptide that strongly inhibits the atypical PKC isoform PKM-zeta but also incompletely inhibits PKC-alpha (62). Our model describes the PKC pathway alongside PKA and CaMKII pathways that are also central for cortical LTP/LTD and is thus well suited to analyze the effects of altered expression of many plasticity-associated proteins on VEP modulation.

It is not known what the circuit mechanisms behind VEPs and their modulation are, but one can safely hypothesize that the modulation-block-induced increase in the VEP amplitude is either due to potentiation of synapses positively contributing to or boosting the VEP amplitude or due to depression of synapses that restrict the VEP amplitude, or both. According to our model and most plasticity data from the cortex, potentiation is typically induced in synapses with GluR1-containing AMPARs and mediated by the PKA pathway, while depression is often induced in synapses with GluR2-containing AMPARs and mediated by the PKC pathway. Our modeling and data analysis showed that SCZ risk genes in the PKA pathway contribute to a statistically significant impairment of the VEP modulation (Figs. 4 *L* and *M* and 5*F*) while the contribution of SCZ risk genes in the PKC pathway was ambiguous and nonsignificant (Figs. 4 *N* and *O* and 5*G*). Our results thus suggest that the SCZ-associated deficit in VEP modulation is due to impairments in the former (potentiation of synapses that positively contribute to VEP-P1) rather than latter (depression of P1-hindering synapses)

type of plasticity. A possible candidate for conveying this effect are L23PCs in the visual cortex: they have been shown to undergo PKA-dependent LTP (28) and are a key population for controlling the cortical output (63)—they also detect a mismatch between visual and top–down inputs (64), which may be relevant in stimulation protocols with abrupt changes such as the checkerboard reversal used in VEP. Substantial contribution to the modulation of VEP may also come from plasticity occurring in other cortical areas, including the ACC (65), one of the two source areas of our differential expression data in SCZ. Although we here tested only the effects of synaptic gene variants on the plasticity induced by the VEP-like protocols, our STDP modeling experiments with altered expression of ion channel-encoding genes (Fig. 3) and the association between the PRS based on ion channel-encoding genes and VEP modulation (Fig. 5*H*) suggest that SCZ-associated alterations in ion channel-encoding gene expression might impair the VEP modulation approximately as strongly as altered expression of synaptic plasticity-regulating genes.

Our results highlighting especially the PKA pathway in the predicted SCZ-associated alterations of plasticity help in narrowing down the generic hypothesis of impaired plasticity in SCZ. Recently, there has been increasing interest toward PDE4 inhibitors as a potential treatment of SCZ. Our results suggest that decreasing PDE4 activity increases the GluR1 membrane insertion and synaptic conductance at baseline and under mild but not strong Ca^{2+} inputs (*SI Appendix*, Fig. S2*C*), leading to an occlusion of HFS-induced LTP in synapses expressing both GluR1 and GluR2 (Fig. 2*K*). Supporting data were obtained in ref. 66, where rolipram, a PDE4 inhibitor, increased the baseline synaptic strength without affecting the maximal synaptic strength attained in an HFS plasticity protocol (although it facilitated LTP in a longer time scale, >2 h after stimulus onset). Thus, the therapeutic effects of PDE4 inhibition may be mediated by increased baseline AMPAR activity and consequently increased basal excitability rather than improved plasticity mechanisms. This is supported by the finding that PDE4 expression is already reduced in SCZ patients (57). Of note, other studies suggest that basal synaptic activity is normal or only mildly strengthened and that the amplitude of early LTP is also enhanced under PDE4 inhibition (67, 68). However, even if PDE4 inhibition may be effective in restoring cognitive functioning in animals and patients where these phenomena are impaired, the small differences in the expression of PDE4 between SCZ and HCs suggest that the cause of the LTP deficits lies somewhere else than in an overexpression of PDE4.

Our model predictions were based on postmortem RNA expression data from two brain regions (PFC and ACC data from the CommonMind), but our framework can be used with other expression data as well when they become available. Indeed, protein expression of the considered genes, especially the ones encoding ion channels and synaptic receptors, can be homeostatically regulated in response to altered expression of other genes that affect excitability or synaptic response (cf. 69). To capture these effects and possible nonlinear cumulative impacts of altered RNA expression, future work should aim to employ protein expression data in addition to the RNA expression data. In our PFC- and ACC-like variants, we included alterations of the concentration of many different proteins based on the RNA expression data but the largest effects on the LTP amplitude were mediated by the expression levels of calcium-dependent intracellular PLA2 (encoded by PLA2G4A, underexpressed in postmortem SCZ brains; see *SI Appendix*, Table S1), RII-type PKA (encoded by PRKAR2A, overexpressed), and the catalytic subunit of PP1 (encoded by PPP1CA or PPP1CC, both underexpressed). Apart from PPP1CC, all these genes were identified using CommonMind data and had relatively low significance in the GWAS data (P-value > 10^{-4}). Another plasticity-regulating gene that has previously been shown to be significant both in GWAS (7, 9) and expression (58) is neurogranin-encoding NRGN. Contribution of variants of this gene to cognitive symptoms is supported by genetic studies that showed an association between SNPs of NRGN and cognitive abilities (70–72). Here, we showed that −20% change in neurogranin expression shifts the LTD/LTP curve leftward (facilitated LTP) and +20% rightward (hindered LTP; Fig. 2*I*). Overexpression of neurogranin was also accompanied by an increase in LTP amplitude for largest Ca^{2+} inputs (>20 Hz stimulation in Fig. 2*I*)—this was in line with experimental data from CA1 (73). The CommonMind datasets predicted an expression difference of up to 6% only, which resulted in very small effects on the threshold and amplitude of LTP (*SI Appendix*, Fig. S3*G*). However, much larger contribution of neurogranin to LTD/LTP could be expected since a decrease of 36 to 72% in neurogranin protein expression, measured by immunostaining, has been observed in postmortem PFCs of SCZ patients (58).

The RNA expression as measured in the CommonMind data is likely to be affected not only by agents causing the disorder (genetic and environmental risk factors) but also by phenomena directly or indirectly caused by the disorder. For example, the use of antipsychotics affects the RNA expression of NMDAR (74) and AMPAR (75, 76) subunits in the rat brain. RNA expression of glutamatergic receptors is also known to be affected by the total level of neural activity through mechanisms of homeostatic regulation (77, 78)—these mechanisms could be expected to occur to adapt to an imbalance of excitation and inhibition, which is believed to occur in many forms in SCZ (79). To avoid these confounds, we left the genes encoding glutamatergic receptor subunits out of our simulations of altered expression although they could be readily included in our modeling framework. As for the genes we included in our modeling framework (*SI Appendix*, Table S1), we did not find evidence of use of antipsychotics or homeostatic regulation affecting the RNA expression. For example, a recent macaque study (80) found RNA expression of many genes affected by antipsychotics use (4 to 56 genes using a P-value threshold of $5 \cdot 10^{-6}$, depending on the type and dose of antipsychotics), but this gene set did not overlap with our modeled genes (*SI Appendix*, Table S1). Likewise, a study on cultured murine cortical neurons showed that lactate stimulation (which is hypothesized to co-occur with increased synaptic activity) alters the RNA expression of 113 plasticity-related genes (81), but none of these was among the ones we used for modeling the effects of SCZ-associated expression alterations (*SI Appendix*, Table S1).

The LTP/LTD pathways in our model are restricted to postsynaptic mechanisms, excluding structural plasticity as well as gene transcription and molecular trafficking between spine and soma. Among the CommonMind-identified genes were CAMK2G (P-value $3 \cdot 10^{-8}$ in PFC and $1 \cdot 10^{-4}$ in ACC), which encodes a CaMKII isoform that, once activated, delivers Ca^{2+}-bound CaM into the nucleus (82) and has been hypothesized to regulate gene transcription (83), and CDK5 (P-value $1 \cdot 10^{-6}$ in PFC and $3 \cdot 10^{-8}$ in ACC), which encodes a cyclin-dependent kinase involved in upregulation of GABAA-receptor activity and suppression of NMDAR clustering (84). Furthermore, among the GWAS-identified genes (8) there are many that directly interact with proteins described in our model, such as the genes encoding protein-phosphatase-regulating sub-

units PPP1R13B, PPP1R16B, PPP2R2A, PPP2R2B, PPP2R3A, PPP2R3C, PPP2R4, PPP2R5B, and PPP3R1 (minimal P-value for SNPs in these genes were $6{\cdot}10^{-14}$, $3{\cdot}10^{-16}$, $8{\cdot}10^{-12}$, $3{\cdot}10^{-6}$, $2{\cdot}10^{-12}$, $6{\cdot}10^{-7}$, $1{\cdot}10^{-6}$, $5{\cdot}10^{-7}$, $1{\cdot}10^{-6}$, respectively). Once the role of these regulatory subunits in protein-phosphatase functioning in neurons is made clear, their contribution to SCZ-associated alterations of plasticity can be studied with our model as well. Furthermore, the effects of a mild-risk SNP of brain-derived neurotrophic factor (BDNF) gene, rs6265, has been widely analyzed in behavioral and electrophysiological experiments and observed to be relevant for SCZ-associated phenotypes (85). While many aspects of the contributions of BDNF to plasticity (dendritic growth and generation of new spines and synapses) cannot be analyzed by our model, the BDNF-mediated exocytosis of GluR1-containing AMPARs could be modeled with a modest extension of our model (addition of TrkB receptors and their coupling to PLC as well as inclusion of IP3R-mediated intracellular Ca^{2+} store release 86). The predictions of our model could also be improved if detailed information on the relative expression of different isoforms of the plasticity-regulating proteins was available.

In conclusion, our results show that the expression alterations observed in SCZ post mortem, especially those in the anterior cingulate cortex, are likely to lead to impaired PKA-pathway-mediated potentiation in synapses containing GluR1 receptors. These results, validated by genomic and electrophysiological data from VEP modulation experiments, provide a possible genetic mechanism for plasticity impairments in SCZ and can form the basis of development of pharmacological treatments.

Materials and Methods

The details of the models and data analysis methods are described in *SI Appendix*. In short, we used biochemically detailed modeling of PKA-, PKC-, and CaMKII-pathway molecules to simulate cortical postsynaptic plasticity using the model of ref. 11. This model was extended to include a description of neurogranin phosphorylation (87) and dephosphorylation (88) and an updated PKC activation scheme (89) (*SI Appendix*, Fig. S9 and section A.1 for details on this extension, and see *SI Appendix*, Tables S3 and S4 for the model reactions and initial conditions, respectively). We adjusted the concentrations of SCZ-associated proteins and explored how the plasticity outcome (poststimulation synaptic conductance normalized by baseline synaptic conductance; see *SI Appendix*, section A.2) was affected. Using the CommonMind postmortem dataset of SCZ patients and HCs, we tested how differences in expression levels of SCZ-associated proteins, as observed in PFC and ACC of SCZ patients, affect the cortical plasticity (*SI Appendix*, section A.3), including STDP (*SI Appendix*, section A.4) and the plasticity induced by VEP-like protocols. To validate our model predictions, we used electrophysiological and genomic data from the TOP Study (36) of 286 HCs. We determined PRSs based on genes relevant for cortical plasticity using the GWAS summary statistics (8) for these subjects and determined the association of these PRSs with the VEP modulation (*SI Appendix*, section A.5). Our model and its implementation in Python with NEURON (RxD) interface as well as scripts for data analyses are publicly available in https://modeldb.science/267741.

Data, Materials, and Software Availability. The simulation scripts (https://modeldb.science/267741) include all codes needed to generate the figures shown in the manuscript, except for those including sensitive expression data (subject-wise RNA expression data). Distribution of the subject-wise data is prohibited by National Institute of Mental Health Data Archive (NDA)–these data are only available to those who have signed the distribution agreement with NDA. For this, only scripts producing population-averaged results (SCZ vs. HC) are included. Likewise, the genetic and electrophysiological data underlying the polygenic risk scores and EEG-VEP data shown in Fig. 5 were sensitive and are not included in the model repository. Previously published data were used for this work (10, 38).

ACKNOWLEDGMENTS. Academy of Finland (330776, 336376, and 318879), University of Oslo Convergence Environment (4MENT), and ERA-NET NEURON project SYNSCHIZ (Research Council of Norway, grant number 283798). CommonMind: Data were generated as part of the CommonMind Consortium supported by funding from Takeda Pharmaceuticals Company Limited, F. Hoffmann-La Roche Ltd. and NIH grants R01MH085542, R01MH093725, P50MH066392, P50MH080405, R01MH097276, RO1-MH-075916, P50M096891, P50MH084053S1, R37MH057881, AG02219, AG05138, MH06692, R01MH110921, R01MH109677, R01MH109897, U01MH103392, and contract HHSN271201300031C through IRP National Institute of Mental Health (NIMH). Brain tissue for the study was obtained from the following brain bank collections: the Mount Sinai NIH Brain and Tissue Repository, the University of Pennsylvania Alzheimer's Disease Core Center, the University of Pittsburgh NeuroBioBank and Brain and Tissue Repositories, and the NIMH Human Brain Collection Core. CMC Leadership: Panos Roussos, Joseph Buxbaum, Andrew Chess, Schahram Akbarian, Vahram Haroutunian (Icahn School of Medicine at Mount Sinai), Bernie Devlin, David Lewis (University of Pittsburgh), Raquel Gur, Chang-Gyu Hahn (University of Pennsylvania), Enrico Domenici (University of Trento), Mette A. Peters, Solveig Sieberts (Sage Bionetworks), Thomas Lehner, Stefano Marenco, and Barbara K. Lipska (NIMH). The authors wish to acknowledge CSC Finland (project 2003397) and Sigma2 Norway (project NN9529K/NS9529K) for computational resources.

Author affiliations: [a]Biomedicine, Faculty of Medicine and Health Technology, Tampere University, Tampere 33720, Finland; [b]Department of Biosciences, University of Oslo, Oslo 0371, Norway; [c]Roy J. Carver Department of Biomedical Engineering, University of Iowa, Iowa City, IA 52242; [d]Norwegian Centre for Mental Disorders Research (NORMENT), Division of Mental Health and Addiction, Oslo University Hospital, Oslo 0450, Norway; [e]Department of Medical Genetics, Oslo University Hospital, Oslo 0450, Norway; [f]K.G. Jebsen Centre for Neurodevelopmental disorders, University of Oslo and Oslo University Hospital, Oslo 0450, Norway; [g]Department of Mental Disorders, Norwegian Institute of Public Health, Oslo 0456, Norway; [h]Department of Neurology, Oslo University Hospital, Oslo 0450, Norway; [i]Department of Physics, Norwegian University of Life Sciences, Ås 1433, Norway; [j]Department of Physics, University of Oslo, Oslo 0316, Norway; and [k]Norwegian Centre for Mental Disorders Research (NORMENT), Institute of Clinical Medicine, University of Oslo, Oslo 0450, Norway

Author contributions: T.M., G.T.E., and O.A.A. designed research; T.M. performed research; K.T.B., I.A., and A.S. contributed new reagents/analytic tools; T.M., K.T.B., I.A., A.S., M.V., T.E., M.-L.L., S.D., G.T.E., and O.A.A. analyzed data; and T.M. wrote the paper.

Competing interest statement: O.A.A. is a consultant to Cortechs.ai and has received speakers honorarium from Lundbeck, Sunovion, Otsuka and Janssen. T.E. is a consultant to Cumulus and Sumitomo Pharma America and received speaker's honoraria from Lundbeck and Janssen Cilag.

1. S. Jauhar, M. Johnstone, P. J. McKenna, Schizophrenia. *Lancet* **399**, 473–486 (2022).
2. R. A. McCutcheon, R. S. Keefe, P. K. McGuire, Cognitive impairment in schizophrenia: Aetiology, pathophysiology, and treatment. *Mol. Psychiatry* **28**, 1–17 (2023).
3. K. E. Stephan, T. Baldeweg, K. J. Friston, Synaptic plasticity and dysconnection in schizophrenia. *Biol. Psychiatry* **59**, 929–939 (2006).
4. A. W. Mould, N. A. Hall, I. Milosevic, E. M. Tunbridge, Targeting synaptic plasticity in schizophrenia: Insights from genomic studies. *Trends Mol. Med.* **27**, 1022–1032 (2021).
5. J. Hall, N. J. Bray, Schizophrenia genomics: Convergence on synaptic development, adult synaptic plasticity, or both? *Biol. Psychiatry* **91**, 709–717 (2022).
6. K. Zhang, P. Liao, J. Wen, Z. Hu, Synaptic plasticity in schizophrenia pathophysiology. *IBRO Neurosci. Rep.* **13**, 478–487 (2022).
7. S. Ripke *et al.*, Biological insights from 108 schizophrenia-associated genetic loci. *Nature* **511**, 421–427 (2014).
8. V. Trubetskoy *et al.*, Mapping genomic loci implicates genes and synaptic biology in schizophrenia. *Nature* **604**, 502–508 (2022).
9. A. Devor *et al.*, Genetic evidence for role of integration of fast and slow neurotransmission in schizophrenia. *Mol. Psychiatry* **22**, 792–801 (2017).
10. G. E. Hoffman *et al.*, Commonmind consortium provides transcriptomic and epigenomic data for schizophrenia and bipolar disorder. *Sci. Data* **6**, 180 (2019).
11. T. Mäki-Marttunen, N. Iannella, A. G. Edwards, G. T. Einevoll, K. T. Blackwell, A unified computational model for cortical post-synaptic plasticity. *eLife* **9**, e55714 (2020).
12. B. Wang, E. Zartaloudi, J. F. Linden, E. Bramon, Neurophysiology in psychosis: The quest for disease biomarkers. *Transl. Psychiatry* **12**, 100 (2022).
13. I. Çavuş *et al.*, Impaired visual cortical plasticity in schizophrenia. *Biol. Psychiatry* **71**, 512–520 (2012).

14. L. Zhong, T. Cherry, C. E. Bies, M. A. Florence, N. Z. Gerges, Neurogranin enhances synaptic strength through its interaction with calmodulin. *EMBO J.* **28**, 3027–3039 (2009).
15. A. Kirkwood, A. Silva, M. F. Bear, Age-dependent decrease of synaptic plasticity in the neocortex of αCaMKII mutant mice. *Proc. Natl. Acad. Sci. U.S.A.* **94**, 3380–3383 (1997).
16. L. Zhong, K. S. Kaleka, N. Z. Gerges, Neurogranin phosphorylation fine-tunes long-term potentiation. *Eur. J. Neurosci.* **33**, 244–250 (2011).
17. Q. S. Fischer *et al*., Requirement for the RIIβ isoform of PKA, but not calcium-stimulated adenylyl cyclase, in visual cortical plasticity. *J. Neurosci.* **24**, 9049–9058 (2004).
18. H. K. Lee, K. Takamiya, K. He, L. Song, R. L. Huganir, Specific roles of AMPA receptor subunit GluR1 (GluA1) phosphorylation sites in regulating synaptic plasticity in the CA1 region of hippocampus. *J. Neurophysiol.* **103**, 479–489 (2010).
19. G. C. Castellani, E. M. Quinlan, F. Bersani, L. N. Cooper, H. Z. Shouval, A model of bidirectional synaptic plasticity: From signaling network to channel conductance. *Learn. Mem.* **12**, 423–432 (2005).
20. J. J. Letzkus, B. M. Kampa, G. J. Stuart, Learning rules for spike timing-dependent plasticity depend on dendritic synapse location. *J. Neurosci.* **26**, 10420–10429 (2006).
21. E. Fino, J. Glowinski, L. Venance, Bidirectional activity-dependent plasticity at corticostriatal synapses. *J. Neurosci.* **25**, 11279–11287 (2005).
22. J. K. Forsyth, D. A. Lewis, Mapping the consequences of impaired synaptic plasticity in schizophrenia through development: An integrative model for diverse clinical features. *Trend. Cogn. Sci.* **21**, 760–778 (2017).
23. H. Z. Shouval, S. S. H. Wang, G. M. Wittenberg, Spike timing dependent plasticity: A consequence of more fundamental learning rules. *Front. Comput. Neurosci.* **4**, 19 (2010).
24. T. Mäki-Marttunen *et al*., Functional effects of schizophrenia-linked genetic variants on intrinsic single-neuron excitability: A modeling study. *Biol. Psychiatry Cogn. Neurosci. Neuroimaging* **1**, 49–59 (2016).
25. T. Mäki-Marttunen *et al*., Pleiotropic effects of schizophrenia-associated genetic variants in neuron firing and cardiac pacemaking revealed by computational modeling. *Transl. Psychiatry* **7**, 5 (2017).
26. T. Mäki-Marttunen *et al*., Computational modeling of genetic contributions to excitability and neural coding in layer V pyramidal cells: Applications to schizophrenia pathology. *Front. Comput. Neurosci.* **13**, 66 (2019).
27. H. Markram *et al*., Reconstruction and simulation of neocortical microcircuitry. *Cell* **163**, 456–492 (2015).
28. G. H. Seol *et al*., Neuromodulators control the polarity of spike-timing-dependent synaptic plasticity. *Neuron* **55**, 919–929 (2007).
29. T. Mäki-Marttunen, V. Mäki-Marttunen, Excitatory and inhibitory effects of HCN channel modulation on excitability of layer V pyramidal cells. *PLoS Comput. Biol.* **18**, e1010506 (2022).
30. K. Obi-Nagata, Y. Temma, A. Hayashi-Takagi, Synaptic functions and their disruption in schizophrenia: From clinical evidence to synaptic optogenetics in an animal model. *Proc. Jap. Acad. Ser. B* **95**, 179–197 (2019).
31. C. Normann, D. Schmitz, A. Fürmaier, C. Döing, M. Bach, Long-term plasticity of visually evoked potentials in humans is altered in major depression. *Biol. Psychiatry* **62**, 373–380 (2007).
32. T. J. Teyler *et al*., Long-term potentiation of human visual evoked responses. *Eur. J. Neurosci.* **21**, 2045–2050 (2005).
33. S. F. Cooke, M. F. Bear, Stimulus-selective response plasticity in the visual cortex: An assay for the assessment of pathophysiology and treatment of cognitive impairment associated with psychiatric disorders. *Biol. Psychiatry* **71**, 487–495 (2012).
34. W. C. Clapp, J. P. Hamm, I. J. Kirk, T. J. Teyler, Translating long-term potentiation from animals to humans: A novel method for noninvasive assessment of cortical plasticity. *Biol. Psychiatry* **71**, 496–502 (2012).
35. N. Zak *et al*., Longitudinal and cross-sectional investigations of long-term potentiation-like cortical plasticity in bipolar disorder type II and healthy individuals. *Transl. Psychiatry* **8**, 1–12 (2018).
36. J. A. Engh *et al*., Delusions are associated with poor cognitive insight in schizophrenia. *Schizophr. Bull.* **36**, 830–835 (2010).
37. M. Valstad *et al*., Experience-dependent modulation of the visual evoked potential: Testing effect sizes, retention over time, and associations with age in 415 healthy individuals. *Neuroimage* **223**, 117302 (2020).
38. M. Valstad *et al*., Evidence for reduced long-term potentiation-like visual cortical plasticity in schizophrenia and bipolar disorder. *Schizophr. Bull.* **47**, 1751–1760 (2021).
39. E. S. Lips *et al*., Functional gene group analysis identifies synaptic gene groups as risk factor for schizophrenia. *Mol. Psychiatry* **17**, 996–1006 (2012).
40. M. Fromer *et al*., Gene expression elucidates functional impact of polygenic risk for schizophrenia. *Nat. Neurosci.* **19**, 1442–1453 (2016).
41. R. C. Roberts, R. Conley, L. Kung, F. J. Peretti, D. J. Chute, Reduced striatal spine size in schizophrenia: A postmortem ultrastructural study. *Neuroreport* **7**, 1214–1218 (1996).
42. J. R. Glausier, D. A. Lewis, Dendritic spine pathology in schizophrenia. *Neuroscience* **251**, 90–107 (2013).
43. M. I. Garrido, J. M. Kilner, K. E. Stephan, K. J. Friston, The mismatch negativity: A review of underlying mechanisms. *Clin. Neurophysiol.* **120**, 453–463 (2009).
44. D. Braff *et al*., Prestimulus effects on human startle reflex in normals and schizophrenics. *Psychophysiology* **15**, 339–343 (1978).
45. T. A. Lett, A. N. Voineskos, J. L. Kennedy, B. Levine, Z. J. Daskalakis, Treating working memory deficits in schizophrenia: A review of the neurobiology. *Biol. Psychiatry* **75**, 361–370 (2014).
46. C. Borralleras *et al*., Synaptic plasticity and spatial working memory are impaired in the cd mouse model of williams-beuren syndrome. *Mol. Brain* **9**, 1–12 (2016).
47. C. S. Chan *et al*., α3-integrins are required for hippocampal long-term potentiation and working memory. *Learn. Mem.* **14**, 606–615 (2007).
48. L. D. Selemon, P. S. Goldman-Rakic, The reduced neuropil hypothesis: A circuit based model of schizophrenia. *Biol. Psychiatry* **45**, 17–25 (1999).
49. S. Akbarian *et al*., Gene expression for glutamic acid decarboxylase is reduced without loss of neurons in prefrontal cortex of schizophrenics. *Arch. Gen. Psychiatry* **52**, 258–266 (1995).
50. M. R. Gluck, R. G. Thomas, K. L. Davis, V. Haroutunian, Implications for altered glutamate and GABA metabolism in the dorsolateral prefrontal cortex of aged schizophrenic patients. *Am. J. Psychiatry* **159**, 1165–1173 (2002).
51. O. B. Smeland, O. Frei, A. M. Dale, O. A. Andreassen, The polygenic architecture of schizophrenia-rethinking pathogenesis and nosology. *Nat. Rev. Neurol.* **16**, 366–379 (2020).
52. P. J. Harrison, Recent genetic findings in schizophrenia and their therapeutic relevance. *J. Psychopharmacol.* **29**, 85–96 (2015).
53. E. Hannon *et al*., Methylation QTLs in the developing brain and their enrichment in schizophrenia risk loci. *Nat. Neurosci.* **19**, 48–54 (2016).
54. A. E. Jaffe *et al*., Mapping DNA methylation across development, genotype and schizophrenia in the human frontal cortex. *Nat. Neurosci.* **19**, 40–47 (2016).
55. O. G. Bhalala, A. P. Nath, M. Inouye, C. R. Sibley, Identification of expression quantitative trait loci associated with schizophrenia and affective disorders in normal brain tissue. *PLoS Genet.* **14**, e1007607 (2018).
56. T. Yoshimizu *et al*., Functional implications of a psychiatric risk variant within *CACNA1C* in induced human neurons. *Mol. Psychiatry* **20**, 162–169 (2015).
57. S. H. Fatemi *et al*., PDE4B polymorphisms and decreased PDE4B expression are associated with schizophrenia. *Schizophr. Res.* **101**, 36–49 (2008).
58. K. Broadbelt, A. Ramprasaud, L. B. Jones, Evidence of altered neurogranin immunoreactivity in areas 9 and 32 of schizophrenic prefrontal cortex. *Schizophr. Res.* **87**, 6–14 (2006).
59. J. J. Straumanis, C. Shagass, R. A. Roemer, Influence of antipsychotic and antidepressant drugs on evoked potential correlates of psychosis. *Biol. Psychiatry* **17**, 1101–1122 (1982).
60. M. Y. Frenkel *et al*., Instructive effect of visual experience in mouse visual cortex. *Neuron* **51**, 339–349 (2006).
61. S. F. Cooke, M. F. Bear, Visual experience induces long-term potentiation in the primary visual cortex. *J. Neurosci.* **30**, 16304–16313 (2010).
62. A. S. Bogard, S. J. Tavalin, Protein kinase C (PKC) ζ pseudosubstrate inhibitor peptide promiscuously binds PKC family isoforms and disrupts conventional PKC targeting and translocation. *Mol. Pharmacol.* **88**, 728–735 (2015).
63. M. Quiquempoix *et al*., Layer 2/3 pyramidal neurons control the gain of cortical output. *Cell Rep.* **24**, 2799–2807 (2018).
64. R. Jordan, G. B. Keller, Opposing influence of top-down and bottom-up input on excitatory layer 2/3 neurons in mouse primary visual cortex. *Neuron* **108**, 1194–1206 (2020).
65. M. S. Sidorov *et al*., Visual sequences drive experience-dependent plasticity in mouse anterior cingulate cortex. *Cell Rep.* **32**, 108152 (2020).
66. V. Wiescholleck, D. Manahan-Vaughan, PDE4 inhibition enhances hippocampal synaptic plasticity in vivo and rescues MK801-induced impairment of long-term potentiation and object recognition memory in an animal model of psychosis. *Transl. Psychiatry* **2**, e89 (2012).
67. M. Barad, R. Bourtchouladze, D. G. Winder, H. Golan, E. Kandel, Rolipram, a type IV-specific phosphodiesterase inhibitor, facilitates the establishment of long-lasting long-term potentiation and improves memory. *Proc. Natl. Acad. Sci. U.S.A.* **95**, 15020–15025 (1998).
68. K. Rutten *et al*., Enhanced long-term potentiation and impaired learning in phosphodiesterase 4D-knockout (PDE4D$^{-/-}$) mice. *Eur. J. Neurosci.* **28**, 625–632 (2008).
69. A. Rátkai *et al*., Homeostatic plasticity and burst activity are mediated by hyperpolarization-activated cation currents and t-type calcium channels in neuronal cultures. *Sci. Rep.* **11**, 3236 (2021).
70. G. Donohoe *et al*., A neuropsychological investigation of the genome wide associated schizophrenia risk variant NRGN rs12807809. *Schizophr. Res.* **125**, 304–306 (2010).
71. A. Krug *et al*., The effect of neurogranin on neural correlates of episodic memory encoding and retrieval. *Schizophr. Bull.* **39**, 141–150 (2013).
72. K. Ohi *et al*., Influence of the NRGN gene on intellectual ability in schizophrenia. *J. Hum. Genet.* **58**, 700–705 (2013).
73. H. Hwang *et al*., Neurogranin, encoded by the schizophrenia risk gene NRGN, bidirectionally modulates synaptic plasticity via calmodulin-dependent regulation of the neuronal phosphoproteome. *Biol. Psychiatry* **89**, 256–269 (2021).
74. M. Krzystanek, A. Pałasz, NMDA receptor model of antipsychotic drug-induced hypofrontality. *Int. J. Mol. Sci.* **20**, 1442 (2019).
75. D. J. Healy, J. H. Meador-Woodruff, Clozapine and haloperidol differentially affect AMPA and kainate receptor subunit mRNA levels in rat cortex and striatum. *Mol. Brain Res.* **47**, 331–338 (1997).
76. X. Guitart *et al*., Regulation of ionotropic glutamate receptor subunits in different rat brain areas by a preferential sigma1 receptor ligand and potential atypical antipsychotic. *Neuropsychopharmacology* **23**, 539–546 (2000).
77. A. C. Penn, A. Balik, C. Wozny, O. Cais, I. H. Greger, Activity-mediated AMPA receptor remodeling, driven by alternative splicing in the ligand-binding domain. *Neuron* **76**, 503–510 (2012).
78. E. Korb, C. L. Wilkinson, R. N. Delgado, K. L. Lovero, S. Finkbeiner, Arc in the nucleus regulates PML-dependent GluA1 transcription and homeostatic plasticity. *Nat. Neurosci.* **16**, 874–883 (2013).
79. C. Kehrer, N. Maziashvili, T. Dugladze, T. Gloveli, Altered excitatory-inhibitory balance in the NMDA-hypofunction model of schizophrenia. *Front. Mol. Neurosci.* **1**, 226 (2008).
80. A. Schulmann *et al*., Antipsychotic drug use complicates assessment of gene expression changes associated with schizophrenia. *Transl. Psychiatry* **13**, 93 (2023).
81. M. B. Margineanu, H. Mahmood, H. Fiumelli, P. J. Magistretti, L-lactate regulates the expression of synaptic plasticity and neuroprotection genes in cortical neurons: A transcriptome analysis. *Front. Mol. Neurosci.* **11**, 375 (2018).
82. H. Ma *et al*., γCaMKII shuttles Ca^{2+}/CaM to the nucleus to trigger CREB phosphorylation and gene expression. *Cell* **159**, 281–294 (2014).
83. H. Ma, B. Li, R. W. Tsien, Distinct roles of multiple isoforms of CaMKII in signaling to the nucleus. *Biochim. Biophys. Acta Mol. Cell Res.* **1853**, 1953–1957 (2015).
84. Z. H. Cheung, A. K. Fu, N. Y. Ip, Synaptic roles of Cdk5: Implications in higher cognitive functions and neurodegenerative diseases. *Neuron* **50**, 13–18 (2006).
85. P. Di Carlo, G. Punzi, G. Ursini, BDNF and schizophrenia. *Psychiatr. Genet.* **29**, 200 (2019).
86. H. Nakata, S. Nakamura, Brain-derived neurotrophic factor regulates AMPA receptor trafficking to post-synaptic densities via IP3R and TRPC calcium signaling. *FEBS Lett.* **581**, 2047–2054 (2007).
87. F. S. Sheu, F. L. Huang, K. P. Huang, Differential responses of protein kinase C substrates (MARCKS, neuromodulin, and neurogranin) phosphorylation to calmodulin and S100. *Arch. Biochem. Biophys.* **316**, 335–342 (1995).
88. K. Seki, H. C. Chen, K. P. Huang, Dephosphorylation of protein kinase C substrates, neurogranin, neuromodulin, and MARCKS, by calcineurin and protein phosphatases 1 and 2A. *Arch. Biochem. Biophys.* **316**, 673–679 (1995).
89. A. R. Gallimore, T. Kim, K. Tanaka-Yamamoto, E. De Schutter, Switching on depression and potentiation in the cerebellum. *Cell Rep.* **22**, 722–733 (2018).